Published in final edited form as:
Environ Sci Technol. 2021 August 17; 55(16): 11265–11273. doi:10.1021/acs.est.1c02220.

Quartz Crystal Microbalance with Dissipation: A New Approach of Examining Corrosion of New Copper Surfaces in Drinking Water

Min Tang [ORISE Postdoctoral Fellow],
Stephen Harmon,
Mallikarjuna N. Nadagouda,
Darren A. Lytle

U.S. Environmental Protection Agency, ORD, CESER, WID, DWMB, Cincinnati, Ohio 45268, United States

Abstract

Corrosion of copper material in drinking water systems causes public health concerns and plumbing failures. This study investigated the early corrosion of new copper surfaces *in situ* using a novel technique: quartz crystal microbalance with dissipation (QCMD). The QCMD results showed that increasing the water pH from 6.5 to 9.0 and the addition of 6 mg/L orthophosphate at pH 6.5 and 9.0 slowed down the copper surface mass changes as indicated by the reduced changes in frequency (Δf5) at 51–89% and total copper release at 29–72%. The water pH 9.0 without orthophosphate was the most likely to induce localized corrosion relative to other conditions at pH 6.5 and pH 9.0 with orthophosphate. Based on the changes in dissipation values (ΔD5) from QCMD and the morphology, microstructure, and composition of the deposited copper corrosion byproducts, digital microscopy, field-emission scanning electron microscopy with energy dispersive spectroscopy, and X-ray photoelectron spectrometry analyses confirmed that the pH and orthophosphate inhibited copper corrosion with different mechanisms. QCMD provided sensitive, rapid, and continuous responses to mass and surface changes and can be useful for evaluating early water corrosivity to new copper.

Graphical Abstract

Corresponding Author: **Darren A. Lytle –** U.S. Environmental Protection Agency, ORD, CESER, WID, DWMB, Cincinnati, Ohio 45268, United States; Phone: 1-513-569-7432; lytle.darren@epa.gov.

Author Contributions

The manuscript was written through contributions of all authors: M. T.: QCMD data collection and analyses and writing manuscript; S. H.: FESEM/EDS data collection and analyses and manuscript edits; M. N. N.: XPS data collection and analyses and manuscript edits; and D. A. L.: Experimental design and manuscript edits. All the authors have approved the final version of the manuscript.

Supporting Information

The Supporting Information is available free of charge at https://pubs.acs.org/doi/10.1021/acs.est.1c02220.

QCMD monitoring apparatus, distribution of change in dissipation, analytical methods of water chemistry parameters, data analyses and calculation example for the QCMD data, digital microscope photos, FESEM/EDS analyses, and XPS analyses (PDF)

Complete contact information is available at: https://pubs.acs.org/10.1021/acs.est.1c02220

The authors declare no competing financial interest.

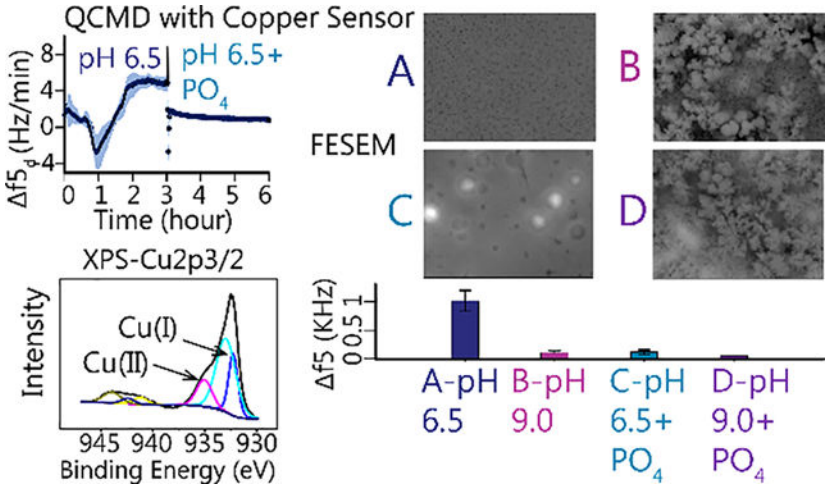

Keywords

quartz crystal microbalance with dissipation (QCMD) monitoring; copper corrosion; water pH; orthophosphate; surface characterization

INTRODUCTION

Copper (Cu) corrosion and associated byproducts in drinking water systems are of concern,[1,2] as they can cause catastrophic building plumbing failures,[3] water aesthetics problems,[4] and human health issues.[5] The morphology, structure, composition, and other characteristics of the inner Cu scale control the nature of corrosion, Cu solubility, and Cu levels in water. It was previously shown that new Cu surfaces exposed to distributed drinking water corrode immediately to form cuprous (Cu(I)) minerals (e.g., Cu_2O and CuOH) next to the surface, and Cu(I) minerals are susceptible to further oxidation to form cupric (Cu(II)) minerals.[2,6,7] Many chemical and physical factors can influence surface mineralogy formation and its associated structure, which ultimately controls the Cu levels in water.[2,7] For instance, aging of Cu plumbing tends to reduce soluble Cu release into water because of its transition from more soluble to less soluble minerals as described by theoretical and field observations.[8–10] In particular, very aged Cu pipes are more likely to bear crystalline and relatively insoluble malachite [$Cu_2CO_3(OH)_2$] or tenorite (CuO) minerals that are in contact with bulk drinking water, whereas newer Cu plumbing tends to have more soluble cupric hydroxide [$Cu(OH)_2$] or georgeite [$Cu_2CO_3(OH)_2{\cdot}6H_2O$] pipe scale.[8–11]

Therefore, early corrosion and associated mineralogical changes of Cu surfaces are extremely important in Cu surface passivation and degradation because of its potential impact on the Cu levels in tap water that are regulated via the Lead and Copper Rule (LCR) via the Safe Drinking Water Act.[8,12] The LCR requires no more than 1.3 mg/L of total Cu in selected home tap water, and adjusting water parameters such as water pH, dissolved inorganic carbon (DIC), and phosphate inhibitors are recommended for Cu surface passivation and reducing total Cu levels in tap water. Previous studies focused on examining the ex situ long-term (up to years) impact of water quality changes and

disruptive events on Cu corrosion cuprosolvency and scale passivation.[13–17] Only a few studies have examined the impact of water pH, phosphate inhibitors, and DIC on the surface roughness, structures, and morphology of the formed nanoscale corrosion byproducts during the early Cu corrosion (<24 h).[18–20] As Cu continues to be commonly used to construct drinking water plumbing in new homes and buildings, a better understanding of early *in situ* interfacial interactions between the drinking water and new Cu surfaces is needed. It can provide insight into the kinetics of early Cu corrosion and immediate Cu surface changes in response to water quality changes.

Quartz (SiO_2) crystal microbalance with dissipation (QCMD) monitoring can continuously capture the *in situ* nanoscale changes resulting from interfacial interactions and chemical reactions over surfaces via monitoring the change of resonating frequency and energy dissipation of a piezoelectric quartz crystal disk with a reasonable time resolution (usually within a few hours).[21–26] The QCMD has been widely applied in diverse fields, and some of the specific areas include studying cell adhesion and spreading,[27,28] membrane permeability,[29] nanoparticle deposition mechanisms under different flowing conditions,[30] detergent efficiency,[31] and biological materials and bioengineered surfaces.[32,33] However, QCMD studies on Cu corrosion in drinking water chemistry are still lacking. Choi first used QCMD to examine the etching or dissolution rate of Cu exposed to deionized water at pH 2.0–10.0, which does not represent the typical drinking water chemistry.[34] Other existing QCMD studies of Cu corrosion were mostly conducted to examine the effect of organic corrosion inhibitors (e.g., benzotriazole, 2,4-dimercapto-pyrimidine, 5-mercapto-1-phenyltetrazole, octadecanethiol, and Cu-dodecanethiol complex) in either aqueous or air phase.[35–39]

QCMD provides an informative insight into early progression and passivation of new Cu surfaces; QCMD appears to be a promising and novel tool for evaluating new Cu pipe-water interactions and reactions in drinking water systems. The objective of this study was to examine the impact of pH and orthophosphate (PO_4) on the corrosion of new Cu surfaces using QCMD. Other complementary surface characterization techniques such as digital microscopy, field-emission scanning electron microscopy with energy dispersive spectroscopy (FESEM/EDS), and X-ray photoelectron spectrometry (XPS) were also used to provide a comprehensive understanding of the QCMD observations.

MATERIALS AND METHODS

Test Water Chemistry.

Five water conditions (designated as A–E) were tested with four water chemistries (A–D) adapted from Daniels et al. (Table S1).[20] Condition A was considered the “baseline” water and had a pH of 6.5, and contained 10 mg C/L DIC, 120 mg SO_4/L sulfate, 60 mg/L chloride, and 3 mg Cl_2/L free chlorine. To examine the impact of water pH and PO_4 on the initial stages of corroding new Cu surfaces, conditions B–D were adjusted as follows: conditions (B) pH 9.0, (C) pH 6.5 with 6 mg/L PO_4 water and (D) pH 9.0 with 6 mg/L PO_4 water. Condition E was initiated with the baseline water during the first half of the experiment immediately followed by the *in situ* addition of 6 mg/L PO_4 to water (pH

remained at 6.5) during the remaining investigation to simulate a water quality change in PO_4.

QCMD Measurements.

The QCMD measurements were conducted on a QSENSE analyzer (Biolin Scientific Q-sense AB, Sweden) with the five water chemistries at a constant flow rate of 150 μL/min (or water flux of 4845 L/(m^2·h)) and at a controlled temperature of 21 °C (Figure S1). The QSENSE analyzer apparatus comprised of an electronics unit (QE 401), a chamber platform (QCP 401) with four flow modules (QFM 401), an Ismatec IPC-N4 pump, and a computer with installed data analysis software (i.e., Qsoft, Qtool, and Dfind). A new Cu sensor (QSX 31313363, NanoScience Instruments) was placed into one flow module immediately after removing the sealed packages per the manufacturer's recommendation. A new Cu sensor was composed of an AT-cut quartz crystal disc base at the bottom followed by 5–10 nm chromium adhesion layer, 100 nm gold layer, 5–10 nm titanium adhesion layer, and lastly, 300 nm Cu layer on the top.

Before pumping the test water over the sensors, the QSENSE analyzer was stabilized in the air for at least 10 min to ensure no drift of frequency (f, Hz) and dissipation (D, 10^{-6}) values. Test waters were pumped via the Ismatec pump over triplicate Cu sensors in parallel for a total of 6 h while measurements were made. Throughout the 6 h experiment, the f and D data for seven overtone numbers (n = 1, 3, 5, 7, 9, 11, and 13) were continuously acquired via the QSoft 401 (v2.7.2). The test water was collected after passing over the sensors for Cu analyses by inductively coupled plasma atomic emission spectroscopy (ICP-AES) (Thermo Elemental, model 6500 duo, Franklin, MA) per EPA Method 200.7.[40] The detection limit for total Cu by ICP-AES was 0.001 mg/L. The analytical methods for other analytes (e.g., pH, chloride, sulfate, PO_4, DIC, and free chlorine) are described in SI-1. After completing each experiment, sensor surfaces were thoroughly dried with nitrogen gas stream before obtaining surface photographs and performing characterization.

Digital Microscopy.

All Cu sensors were photographed using a digital reflective light microscope (VHX-600) under 20× and 100× magnification before and after each experiment to identify and document Cu surfaces' changes.

Field-Emission Scanning Electron Microscopy with Energy Dispersive Spectroscopy.

A Japan Electron Optics Laboratory (JEOL) 7600 FESEM (Tokyo, Japan) was used to image the structure and morphology on the surface of experimental Cu sensors under 500–10,000× magnifications. EDS also provided a semiquantitative measurement of elemental composition of formed corrosion byproducts on sensor surfaces via an Oxford Instruments (Abingdon, United Kingdom) 50 mm^2 X-Max silicon drift detector and Aztec v.3.3 SP1 software.

X-ray Photoelectron Spectroscopy.

The oxidation state of essential elements on a representative Cu sensor surface (i.e., one of the triplicates) for each water condition was examined using XPS. XPS measurements were

obtained by a Kratos Axis Ultra XPS equipped with a monochromated (Al) X-ray source (12 kV and 10 mA) in a spectrum analyzer mode and slot aperture setting with a hybrid lens mode. Samples were pressed on a carbon tape (~1 cm^2) and taped on a metal sample holder. Comprehensive survey scans were obtained first followed by core-level peaks (e.g., C1s, O1s, N1s, Al2p, Cu2p 3/2, Cl2p, S2p, and P2p) in detail that targeted present vital elements.

QCMD Data Analysis.

Smaller overtone numbers (n = 3, 5, and 7) corresponding to a larger active surface area have been reported to give more consistent results,[22,41] and therefore, these overtone numbers were examined for this study and showed comparable results. For illustration purposes, the f and D data for n = 5 (i.e., f5 and D5) were presented.

First, the kinetics of Cu corrosion was monitored over time using the distribution of changes in f5 (i.e., changes of f5 every minute or denoted as $\Delta f5_d$) (Calculation S1). Numerous studies indicated that changes in f (Δf) provide qualitative information about dynamic changes over the surface, and that increase in Δf corresponds to a decrease in accumulated mass on the surface.[23,24,27–29,31–33] The increase in mass could be attributed to the accumulation of Cu(I) and Cu(II) corrosion byproducts and/or deposition of other minerals on the Cu sensor surface. In our study, it was impossible to distinguish the specific source of mass increase; however, given the simplicity of the test water makeup, it was unlikely that solids other than Cu corrosion byproducts would precipitate under the experimental conditions over the surface. In this case, an increase in $\Delta f5_d$ indicated a faster loss of Cu, whereas a decrease in $\Delta f5_d$ indicated a slower Cu loss. The total Cu loss included Cu(I) and Cu(II) species. Second, the temporal trend of Δf5 and total Cu release were jointly presented to semiquantitatively compare the overall Cu mass changes at different water conditions. Third, the change in dissipation (ΔD5) data representing changes in the sensor surface properties was compared and linked to the results by other surface characterization techniques, including digital microscopy, FESEM/EDS, and XPS. Fourth, as Δf and ΔD only gave a semiquantitative and qualitative measure of Cu corrosion processes, the acquired f and D data in Qsoft401 were exported to Qsense Dfind (v1.2.6). Two well-established models including Sauerbrey and viscoelastic models for quantifying mass changes over Cu surfaces were tested. The two models have been used in many applications and the assumptions and equations for the two models are detailed in SI-2.

Briefly, the Sauerbrey model indicates that the changes in mass (Δm) on the quartz surface are linearly correlated to Δf of the oscillating crystal (eq 1).[21] The Sauerbrey model has shown to be accurate for nanoscale changes in a laterally homogenous film, a monolayer of discrete particles, or other nanosized objects.[26] For deposited small size particles, a direct response for conditions following the Sauerbrey relation is a low dispersion in $\Delta f_n/n$ at a given overtone number or minimal ΔD.[26] In cases where Δm exhibited a frequency and an overtone number-dependent relationship and the $\Delta D/n$ and $\Delta f/n$ values do not overlay for all overtone numbers with usually a large ΔD, the two-layer viscoelastic Voight model was used to analyze the data.[42] For both models, a high-model estimate fit of close to 1 indicates a suitable model for quantifying the nanoscale mass changes of the new Cu surface, and a low-model fit estimate of close to 0 indicates the opposite

$$\Delta f = -n\frac{\Delta m}{C} \quad (1)$$

where f is the resonance frequency of quartz plate, Δm is the mass change per active area of quartz plate, n is the harmonic overtone number (1, 3, 5, 7, 9,11, and 13), and C is a constant 17.7 ng cm^{-2} Hz^{-1} for quartz with a fundamental resonance frequency of 5 MHz.

RESULTS AND DISCUSSION

Kinetics, and total surface mass changes, and its associated physicochemical changes of new Cu surfaces exposed to five test waters were examined using QCMD, coupled with digital microscopy, FESEM/EDS, and XPS techniques.

Kinetics of Cu Surface Mass Changes as a Function of Time.

The distribution of Δf5 (designated as $\Delta f5_d$) was calculated to compare the kinetics of Cu mass changes. For these five water conditions, the kinetics of Cu mass changes varied depending on the water quality (Figure 1).

After triplicate Cu sensors were exposed to the baseline water at pH 6.5 (condition A) for 6 h, the average $\Delta f5_d$ for the triplicate Cu sensors decreased from 4.7 ± 0.9 Hz/min at the start to −0.27 ± 1.8 Hz/min at 111 min; after 117 min the average $\Delta f5_d$ increased to above zero and up to 5.9 ± 1.8 Hz/min after 6 h (Figure 1). The rate of Cu loss from the sensor surface decreased in the first 111 min, presumably because of the passivation of Cu corrosion byproducts; afterward, the Cu loss started to dominate and continued to increase during the remaining exposure time.

In contrast, conditions B–D representing pH 9.5 water, pH 6.5 with 6 mg/L PO_4 water, and pH 9.0 with 9 mg/L PO_4 water, respectively, exhibited different patterns, and that the kinetics of Cu mass changes decreased rapidly in the first 10 min and then remained steady for the remainder of test (Figure 1). A comparison between conditions A and B–D revealed that increasing pH or the addition of PO_4 rapidly slowed the oxidation and/or enhanced the passivation of the Cu surface. The beneficial impact of PO_4 was obvious in condition E that simulated a water quality change by adding PO_4 after prerun with the baseline water. The $\Delta f5_d$ sharply decreased from 5 Hz/min down to 1 Hz/min within 60 min after PO_4 was introduced.

Measure of Total Cu Surface Mass Changes by Changes in Frequency.

For all the five tested conditions, Δf5 showed an upward trend, semiquantitatively indicating an overall loss of Cu mass from the sensor surface (Figure 2). As indicated by the slower kinetics of Cu mass release (Figure 1), increasing water pH and the addition of PO_4 also reduced the overall Δf5 and Cu mass loss from the sensor surface (Figure 3a,b).

The average Δf5 for the baseline water (condition A) increased up to 1012 ± 182 Hz by the end of the 6 h exposure (Figure 3a). During this time, a total of 28 ± 1.3 μg Cu was released

from the sensor surface based on water quality measurements (Figure 3b). In contrast, the average Δf5 was decreased by 89, 88, and 95% for the pH 9.5 water (condition B), pH 6.5 with 6 mg/L PO_4 water (condition C), and pH 9.0 with 6 mg/L PO_4 water (condition D), resulting in 113 ± 27, 120 ± 36, and 54 ± 1.8 Hz, respectively. The total Cu release for conditions B–D was also 51, 29, and 83% lower than that in the baseline water, respectively. For condition E, the addition of PO_4 after the initial stages of corrosion was allowed to precede under the baseline water condition that decreased Δf5 by 51% and the total Cu release by 72%, again demonstrating that PO_4 affected the oxidation and/or passivation of the Cu surface.

Linking Dissipation to Mechanistic Understanding of Cu Surface Corrosion.

The *in situ* Cu surface changes due to Cu dissolution, deposition of associated byproducts, and other processes associated with Cu corrosion were also observed and reflected by ΔD5, a sum of $\Delta D5_d$ (Figure S2). The ΔD5 exhibited an upward trend for conditions A–C (Figure 2) and the average ΔD5 increased up to $3.7 \times 10^{-6} \pm 2.2 \times 10^{-6}$, $56 \times 10^{-6} \pm 19 \times 10^{-6}$, and $59 \times 10^{-6} \pm 45 \times 10^{-6}$, respectively (Figure 3c). The changes in ΔD5 were previously shown to indicate changes in shear viscosity, elastic shear modulus properties, and thickness of Cu surfaces that resulted from direct hydration reactions, viscous drag interactions, and entrapment of aqueous molecules in cavities of formed films.[42] The condition D water at pH 9.5 with 6 mg/L PO_4 was an exception, and the average D5 was very low at $0.3 \times 10^{-6} \pm 0.4 \times 10^{-6}$, implying a minimal change of viscoelastic properties of Cu surfaces (Figure 3c).

Interestingly, although the addition of PO_4 to pH 6.5 from the start (condition C) increased ΔD5 by 1495% on average when compared to the baseline, the addition of PO_4 after prerun with the baseline water (condition E) decreased ΔD5 by 17% (Figure 3c). This implied that the order of PO_4 addition and increasing water pH might have fundamentally changed the morphology, structure, composition, and other properties of the sensor surface. Surface characterizations by digital microscopy, FESEM/EDS, and XPS techniques further confirmed the changes of Cu surface properties under different water conditions.

When viewed by digital reflective light microscopy, the Cu sensor surface was examined in macroscale (Figure S3). The sensor surface exposed to baseline water (condition A) was fully covered with very fine-grained blue, green, and purple corrosion deposits. The direction of water flow was evident on some of the deposits, and apparent signs of pitting had developed in some areas. When exposed to water at higher pH (condition B), brown, green, and off-white deposits appeared locally on the surface and covered a small surface area suggesting localized corrosion. For condition C with PO_4 added at pH 6.5 from the start, the sensor surface was fully covered with reddish-brown to off-white massive deposits. For condition D with PO_4 added at higher pH 9.0, small surface areas were covered with white and light-yellow corrosion byproducts. For condition E with PO_4 added after prerun with the baseline water, the appearance of the green, brown, and blue Cu corrosion byproducts over the Cu sensor was very similar to those in condition A.

The higher magnification examination of the surface morphology via FESEM showed microscale changes in the structure and morphology of Cu sensor surfaces (Figures 4 and S4–S9). For baseline condition A, the Cu surface exhibited various grain textures

from massive to granular (Figures 4 and S5). There appeared to be a secondary, irregular grid-like microstructure developed in some deposits. For condition B at higher pH, localized corrosion appeared to attack and penetrate through the top 300 nm Cu layer of the sensor below the bladed and tabular flowerlike microscale deposits (Figures S6). The observation was consistent with the past long-term work which found that the extent of nonuniform corrosion was more severe at high pH, low DIC, and chlorinated water.[43–45] For condition C with PO_4 added at pH 6.5, the massive deposits were observed lacking other fine structures seen in the baseline condition (Figure 4). This surface showed signs of possible pitting in localized areas. One localized attack resulted in penetration through the top Cu layer of the sensor and exposed the gold layer to the testing water (Figure S7). For condition D with PO_4 added at pH 9.0, the microscale deposits were semibotryoidal to bladed and tabular flowerlike and the surface was attacked to a relatively smaller extent in both area coverage and penetration depth relative to conditions A–C (Figures 4 and S8). This was consistent with findings by Lytle and Schock that PO_4 prevented a localized attack in low DIC and high pH water.[43] For condition E with PO_4 added after prerun with the baseline water, unlike the relatively large deposits in condition C, deposits on the Cu sensor surface had microscale subhedral-bladed grains (Figure S9).

The EDS analysis indicated the elemental composition over the Cu surface (Figures 4 and S5–S10). XPS analysis of higher precision than EDS could detect trace levels of elements and provided the primary functional sites and the surface valence states of elements over the Cu surface (Figures S11–S15). For conditions A and B that had no addition of PO_4, the surface deposits contained Cu, oxygen, carbon, and a trace amount of elemental chlorine and sulfur after combining EDS and XPS analyses results (Figures S5,S6, and S10). Although for conditions C–E that had addition of PO_4, the surface deposits also incorporated additional phosphorus (Figures S7–S9).

Additionally, the XPS analysis demonstrated that Cu corrosion byproducts for all conditions consisted of a combination of Cu(I) and Cu(II) minerals (Figure 5). In particular, in the spectrum of Cu 2p3/2, each valence of targeted element was assigned with peaks at different binding energies. For instance, for one replicate sensor in condition A, in the Cu2p spectrum, two peaks at 934.4 and 932.2 eV could be assigned to Cu(II) and Cu(I), respectively (Figure 5). The peaks at 934.4 eV with the satellite peaks at 941.0 and 943.8 eV corresponded to Cu2p 3/2 [Cu(II)]. Similar analyses were then conducted for O1, Cl2p, S2p, and P2p spectrums (Figures S11–S15). As an example, for condition A, in Cl2p spectrum, peaks at 198.2 and 199.7 eV corresponded to chloride $3p_{3/2}$ and chloride $2p_{1/2}$. In the O1s spectrum, peaks at 530.4, 531.2, and 531.9 eV could be assigned to lattice oxygen (Cu–O), hydroxyl oxygen, and adsorbed oxygen, respectively (Figure S11). Therefore, the Cu deposits for condition A were in the form of Cu(I) and Cu(II) oxides, hydroxides, chloride, and sulfate. Condition B had similar minerals to condition A, and conditions C–E incorporated additional Cu(I) and Cu(II) phosphate minerals (Figures S12–S15).

The above in-depth sensor surface analyses validated that increasing water pH, PO_4 addition, and order of PO_4 addition altered the nature of the corrosion byproducts over the Cu surface. Adding PO_4 from the start in condition C had different interactions with the

new Cu surface from that with the used Cu surface covered with Cu(I) and Cu(II) deposits in condition E.

Testing Sauerbrey and Viscoelastic Models.

To test whether the established Sauerbrey and viscoelastic models were appropriate to quantify mass changes over the Cu surfaces, the model fit estimate was provided (Figure 3d). The viscoelastic model failed to quantify mass changes for all conditions as indicated by a very low model estimate of 0.000–0.007. Meanwhile, the Sauerbrey relation was not appropriate for conditions A–C and E with the model estimate fit at 0.007–0.23. However, the Sauerbrey relation seemed suitable for modeling mass changes for condition D, which was shown to the least corrosive to new Cu by the above analyses. The estimated Sauerbrey model fit for condition D was at 1.0, indicating that the mass changes were in nanoscale and that the spreading of the frequency at different overtone numbers was minimal. As the Cu sensors with conditions A–C and E underwent large Δf, which was 2–3 orders of magnitude higher than those reported in previous QCMD studies of Cu corrosion,[35–39] it was likely that the large mass changes in conditions A–C and E might have failed the assumption that requires nanoscale mass changes. Our results suggested that the established Sauerbrey and viscoelastic models might not be applicable to certain experimental conditions and should only be used after proper verification. Using other methods to directly quantify the mass changes over the Cu sensor surface and then relating them to the measured Δf and ΔD and modeled Δm seemed appropriate to carry out for verification. Existing high-precision characterization and analytical tools such as XPS, ICP-MS, and laboratory balance were attempted and were not able to track nanoscale mass changes over sensor surfaces. It is worth conducting further verification in the future as new tools are developed.

Discussion.

This was the first QCMD study to examine the relative degree and kinetics of mass changes and their associated property surface changes of new Cu during the early stages of corrosion in water. Although Sauerbrey and viscoelastic models were not always appropriate for quantifying mass changes taking place on new Cu surfaces, the $\Delta f5_d$, $\Delta f5$, and $\Delta D5$ QCMD data clearly revealed the impact of water pH and PO_4 on newly corroded Cu. The observations were consistent with coupled surface characterization methods (digital microscopy, FESEM/EDS, and XPS) applied to the Cu surfaces.

The QCMD analyses showed that both increasing water pH from 6.5 to 9.0 and the addition of 6 mg/L PO_4 at a water pH of 6.5 and 9.0 effectively inhibited Cu mass changes. The mass changes corresponded to physiochemical changes on Cu surfaces based on QCMD measurements, which was also in agreement with observations of early Cu corrosion in water by others.[18–20] Previous studies, for example, showed that increasing water pH reduced Cu release by reducing the solubility of Cu corrosion byproducts deposited on the surface via influencing the diffusion process from the passivating film layer.[8,46,47]

Defining the specific pathway(s) and mechanism(s) associated with the role of PO_4 on Cu corrosion remains a challenge; however, several roles have been proposed that are consistent with this research. For example, the addition of PO_4 might alter the nature of the passivating

film by interfering with the surface scale oxidation, passivation, and aging processes.[8,46,48–51] Alternatively, it has been suggested that the negatively charged PO_4 was adsorbed on the Cu anodic sites, thereby blocking the active sites and slowing down the dissolution of Cu.[46,48] Yet in another mechanism, others have indicated that the oxidation of Cu(I) was inhibited by PO_4 while PO_4 was incorporated into the Cu scale and the newly formed products controlled and reduced the solubility of Cu in water.[50,51]

It was not possible to identify which potential mechanism(s) play a role in the experimental observations, but it was likely that PO_4 reduced the total Cu mass changes and Cu solubility dominantly by slowing down Cu(I) oxidation and scale incorporation for condition E where there were existing Cu(I) and Cu(II) deposits following the PO_4 addition. In contrast, PO_4 likely reduced the mass changes and Cu solubility dominantly via the PO_4 adsorption mechanism for conditions C–D when PO_4 was added from the start.

The QCMD analyses coupled with materials surface characterization observations provided confirmational and supplemental results regarding the details on the nature of the very early stages of Cu corrosion for the evaluated water chemistries. For example, the higher pH of 9.0 without PO_4 induced a higher observation of localized corrosion, whereas the addition of PO_4 to pH 9.0 water tended to reduce the localized corrosion tendency. Lower pH 6.5 water reduced the localized corrosion tendencies; however, greater Cu release was observed. Although this work was very short term, the results suggest that waters that initiate high Cu release and cause localized Cu corrosion essentially exhibited different water characteristics, which has been reported in previous long-term Cu studies.[8,14,15,43,49]

Implication.

This work showed that the novel QCMD tool was useful to monitor real-time changes that occurred on new Cu surfaces resulting from dissolution, passivation, and other processes. The QCMD uniquely provided rapid and sensitive responses to surface changes associated with corroding Cu surfaces and the ability to evaluate the impact of water quality changes *in situ*. The use of QCMD is of interest to the water industry, particularly when coupled with complementary surface characterization tools, in which the QCMD could provide an important insight into water corrosivity to the new Cu surface and initiation of localized corrosion.

Supplementary Material

Refer to Web version on PubMed Central for supplementary material.

ACKNOWLEDGMENTS

This project was supported in part by appointment to the Research Participation Program at the U.S. Environmental Protection Agency Office of Research and development, administered by the Oak Ridge Institute for Science and Education (ORISE), Oak Ridge, Tennessee, through an interagency agreement between the U.S. Department of Energy and U.S. EPA. The authors acknowledge Jennifer Tully (U.S. EPA) for helping with early SEM work. The authors acknowledge Christy Muhlen and Daniel Williams from U.S. EPA for helping set up the experimental apparatus. The authors acknowledge Megan Raisle (former ORISE intern at U.S. EPA) for helping with the graphics. The authors thank Matt Dixon and Archana Jaiswal from NanoScience Instrument for assisting with QCM-D data interpretation and analyses. The authors also acknowledge Mike DeSantis and Andrea Porter from U.S. EPA for critically reviewing this manuscript and providing insightful comments.

Funding

The U.S. Environmental Protection Agency, through its Office of Research and Development, funded the research described herein. It has been subjected to the Agency's peer and administrative review and has been approved for external publication. Any opinions expressed in this paper are those of the author(s) and do not necessarily reflect the Agency's views. Therefore, no official endorsement should be inferred. Any mention of trade names or commercial products does not constitute endorsement or recommendation for use.

ABBREVIATIONS

LCR	Lead and Copper Rule
DIC	dissolved inorganic carbon
QCMD	quartz crystal microbalance with dissipation
FESEM/EDS	field-emission scanning electron microscopy with energy dispersive spectroscopy
XPS	X-ray photoelectron spectrometry
ICP-AES	inductively coupled plasma atomic emission spectroscopy

REFERENCES

(1). Critchley MM; Cromar NJ; McClure N; Fallowfield HJ Biofilms and microbially influenced cuprosolvency in domestic copper plumbing systems. J. Appl. Microbiol 2001, 91, 646–651. [PubMed: 11576301]

(2). Vargas I; Fischer D; Alsina M; Pavissich J; Pastén P; Pizarro G Copper corrosion and biocorrosion events in premise plumbing. Dent. Mater 2017, 10, 1036.

(3). Scardina P; Edwards M; Bosch DJ; Loganathan GV; Dwyer SK Assessment of non-uniform corrosion in copper piping; American Water Works Association Research Foundation: Denver, CO, 2008.

(4). Edwards M; Jacobs S; Taylor RJ The blue water phenomenon. J. Am. Water Work. Assoc 2000, 92, 72–82.

(5). Dietrich AM; Glindemann D; Pizarro F; Gidi V; Olivares M; Araya M; Camper A; Duncan S; Dwyer S; Whelton AJ; Younos T Health and aesthetic impacts of copper corrosion on drinking water. Water Sci. Technol 2004, 49, 55–62.

(6). Ives DJG; Rawson AE Copper corrosion: III. electrochemical theory of general corrosion. J. Electrochem. Soc 1962, 109, 458.

(7). Merkel TH; Pehkonen SO General corrosion of copper in domestic drinking water installations: scientific background and mechanistic understanding. Corros. Eng., Sci. Technol 2006, 41, 21–37.

(8). Schock MR; Lytle DA; Clement JA Effect of pH, DIC, orthophosphate and sulfate on drinking water cuprosolvency; US EPA: Office of Research and Development: Washington, DC, 1995, No. PB-95-269270/XAB; EPA-600/R-95/085.

(9). Edwards M; Powers K; Hidmi L; Schock MR The role of pipe ageing in copper corrosion by-product release. Water Supply 2001, 1, 25–32.

(10). Turek NF; Kasten L; Lytle DA; Goltz MN Impact of plumbing age on copper levels in drinking water. J. Water. Supply. Res. T 2011, 60, 1–15.

(11). Lytle DA; Wahman DG; Schock MR; Nadagouda MN; Harmon S; Webster K; Botkins J Georgeite: a rare copper mineral with important drinking water implications. Chem. Eng. J 2019, 355, 1–10. [PubMed: 31275053]

(12). United States Environmental Protection Agency (US EPA). National primary drinking water regulations: lead and copper rule revisions. Fed. Regist 2021, 86, 4198–4312.

(13). Schock MR; Sandvig AM Long-term effects of orthophosphate treatment on copper concentration. J. Am. Water Work. Assoc 2009, 101, 71–82.

(14). Edwards M; Meyer T; Rehring J Effect of selected anions on copper corrosion rates. J. Am. Water Work. Assoc 1994, 86, 73–81.

(15). Edwards M; Schock MR; Meyer TE Alkalinity, pH, and copper corrosion by-product release. J. Am. Water Work. Assoc 1996, 88, 81–94.

(16). Edwards M; Jacobs S; Dodrill D Desktop guidance for mitigating Pb and Cu corrosion by-products. J. Am. Water Work. Assoc 1999, 91, 66–77.

(17). American Water Works Association Research Foundation (AWWARF). Internal Corrosion of Water Distribution Systems; 2nd edition, AwwaRF/DVGW-TZW: Denver, CO, 1996.

(18). Lewandowski BR; Lusker KL; LeJeune Z; Lytle DA; Zhou P; Sprunger P; Garno JC Impact of pH, dissolved inorganic carbon, and polyphosphates for the initial stages of water corrosion of copper surfaces investigated by AFM and NEXAFS. Corros. Sci 2011, 1, 16–26.

(19). Lewandowski BR; Lytle DA; Garno JC Nanoscale investigation of the impact of pH and orthophosphate on the corrosion of copper surfaces in water. Langmuir 2010, 26, 14671–14679. [PubMed: 20799694]

(20). Daniels SL; Sprunger PT; Kizilkaya O; Lytle DA; Garno JC Nanoscale surface characterization of aqueous copper corrosion: effects of immersion interval and orthophosphate concentration. Appl. Surf. Sci 2013, 285, 823–831.

(21). Sauerbrey GZ The use of quarts oscillators for weighing thin layers and for microweighing. Z. Phys 1959, 155, 206–222.

(22). Hök F; Rodahl M; Brzezinski P; Kasemo B Energy dissipation kinetics for protein and antibody–antigen adsorption under shear oscillation on a quartz crystal microbalance. Langmuir 1998, 14, 729–734.

(23). Hök F; Kasemo B; Nylander T; Fant C; Sott K; Elwing H Variations in coupled water, viscoelastic properties, and film thickness of a Mefp-1 protein film during adsorption and cross-linking: a quartz crystal microbalance with dissipation monitoring, ellipsometry, and surface plasmon resonance study. Anal. Chem 2001, 73, 5796–5804. [PubMed: 11791547]

(24). Rodahl M; Hök F; Krozer A; Brzezinski P; Kasemo B Quartz crystal microbalance setup for frequency and Q-factor measurements in gaseous and liquid environments. Rev. Sci. Instrum 1995, 66, 3924–3930.

(25). Rodahl M; Kasemo B A simple setup to simultaneously measure the resonant frequency and the absolute dissipation factor of a quartz crystal microbalance. Rev. Sci. Instrum 1996, 67, 3238–3241.

(26). Reviakine I; Johannsmann D; Richter RP Hearing what you cannot see and visualizing what you hear: interpreting quartz crystal microbalance data from solvated interfaces. Anal. Chem 2011, 83, 8838–8848. [PubMed: 21939220]

(27). Chen JY; Penn LS; Xi J Quartz crystal microbalance: Sensing cell-substrate adhesion and beyond. Biosens. Bioelectron 2018, 99, 593–602. [PubMed: 28830033]

(28). Gutman J; Walker SL; Freger V; Herzberg M Bacterial attachment and viscoelasticity: physicochemical and motility effects analyzed using quartz crystal microbalance with dissipation (QCM-D). Environ. Sci. Technol 2013, 47, 398–404. [PubMed: 23186151]

(29). Liu SX; Kim JT Study of adsorption kinetics of surfactants onto polyethersulfone membrane surface using QCM-D. Desalination 2009, 247, 355–361.

(30). Kim C; Pennell KD; Fortner JD Delineating the relationship between nanoparticle attachment efficiency and fluid flow velocity. Environ. Sci. Technol 2020, 54, 13992–13999. [PubMed: 33052644]

(31). Olesen K; Van Leeuwen C; Andersson FI Revealing detergent efficiency and mechanism by real-time measurement using a novel and tailored QCM-D methodology. Tenside Surfactant Deterg. 2016, 53, 488–494.

(32). Dixon MC Quartz crystal microbalance with dissipation monitoring: enabling real-time characterization of biological materials and their interactions. J. Biomol. Tech 2008, 19, 151. [PubMed: 19137101]

(33). Tonda-Turo C; Carmagnola I; Ciardelli G Quartz crystal microbalance with dissipation monitoring: a powerful method to predict the in vivo behavior of bioengineered surfaces. Front. Bioeng. Biotechnol 2018, 6, 158. [PubMed: 30425985]

(34). Choi C Kinetic Study Of Copper Chemistry In Chemical Mechanical Polishing (CMP) By An In-Situ Real Time Measurement Technique. PhD Dissertation: Iowa State University, 2008.

(35). Fonsati M; Zucchi F; Trabanelli G Study of corrosion inhibition of copper in 0.1 M NaCl using the EQCM technique. Electrochim. Acta Theriol 1998, 44, 311–322.

(36). Galvani CM; Graydon A; Riley DJ; York D Electrochemical quartz crystal microbalance in a channel flow cell: a study of copper dissolution. J. Phys. Chem. C 2007, 111, 3669–3674.

(37). Schwind M; Hosseinpour S; Johnson CM; Langhammer C; Zorić I; Leygraf C; Kasemo B Combined in situ quartz crystal microbalance with dissipation monitoring, indirect nanoplasmonic sensing, and vibrational sum frequency spectroscopic monitoring of alkanethiol-protected copper corrosion. Langmuir 2013, 29, 7151–7161. [PubMed: 23713406]

(38). Niu S; Fang Y; Qiu R; Qiu Z; Xiao Y; Wang P; Chen M Superhydrophobic film based on Cu-dodecanethiol complex: Preparation and corrosion inhibition for Cu. Colloids Surf. A Physicochem. Eng. Asp 2018, 550, 65–73.

(39). Wu B; Raghavan S Removal of BTA adsorbed on Cu: a feasibility study using the quartz crystal microbalance with dissipation (QCMD) technique. ECS J. Solid State Sci. Technol 2019, 8, P3114–P3117.

(40). United States Environmental Protection Agency (US EPA). Methods For The Determination Of Metals In Environmental Samples; EPA-600/4–91–010, Washington, DC, 1994.

(41). Hovgaard MB; Dong M; Otzen DE; Besenbacher F Quartz crystal microbalance studies of multilayer glucagon fibrillation at the solid-liquid interface. Biophys. J 2007, 93, 2162–2169. [PubMed: 17513349]

(42). Voinova MV; Rodahl M; Jonson M; Kasemo B Viscoelastic acoustic response of layered polymer films at fluid-solid interfaces: continuum mechanics approach. Phys. Scr 1999, 59, 391.

(43). Lytle DA; Schock MR Pitting corrosion of copper in waters with high pH and low alkalinity. J. Am. Water Work. Assoc 2008, 100, 115–129.

(44). Lytle DA; Williams D; White C A simple approach to assessing copper pitting corrosion tendencies and developing control strategies. J. Water. Supply. Res. T 2012, 61, 164–175.

(45). Sarver E; Dodson K; Scardina RP; Lattyak-Slabaugh R; Edwards M; Nguyen C Copper pitting in chlorinated, high-pH potable water. J. Am. Water Work. Assoc 2011, 103, 86–98.

(46). Dartmann J; Sadlowsky B; Dorsch T; Johannsen K Copper corrosion in drinking water systems–effect of pH and phosphate-dosage. Mater. Corros 2010, 61, 189–198.

(47). Feng Y; Siow KS; Teo WK; Tan KL; Hsieh AK Corrosion mechanisms and products of copper in aqueous solutions at various pH values. Corrosion 1997, 53, 389–398.

(48). Uhlig HH; Revie RW Corrosion And Corrosion Control; Third edition, United States, 1985.

(49). Lytle D Copper corrosion: copper release to pitting corrosion. Office of Research and Development and Office of Water, U.S Environmental Protection Agency, February 23, 2021. Available online at: https://www.epa.gov/water-research/small-drinking-water-systems-webinar-series.

(50). Valcarce MB; Vázquez M Phosphate ions used as green inhibitor against copper corrosion in tap water. Corros. Sci 2010, 52, 1413–1420.

(51). Edwards M; Hidmi L; Gladwell D Phosphate inhibition of soluble copper corrosion by-product release. Corros. Sci 2002, 44, 1057–1071.

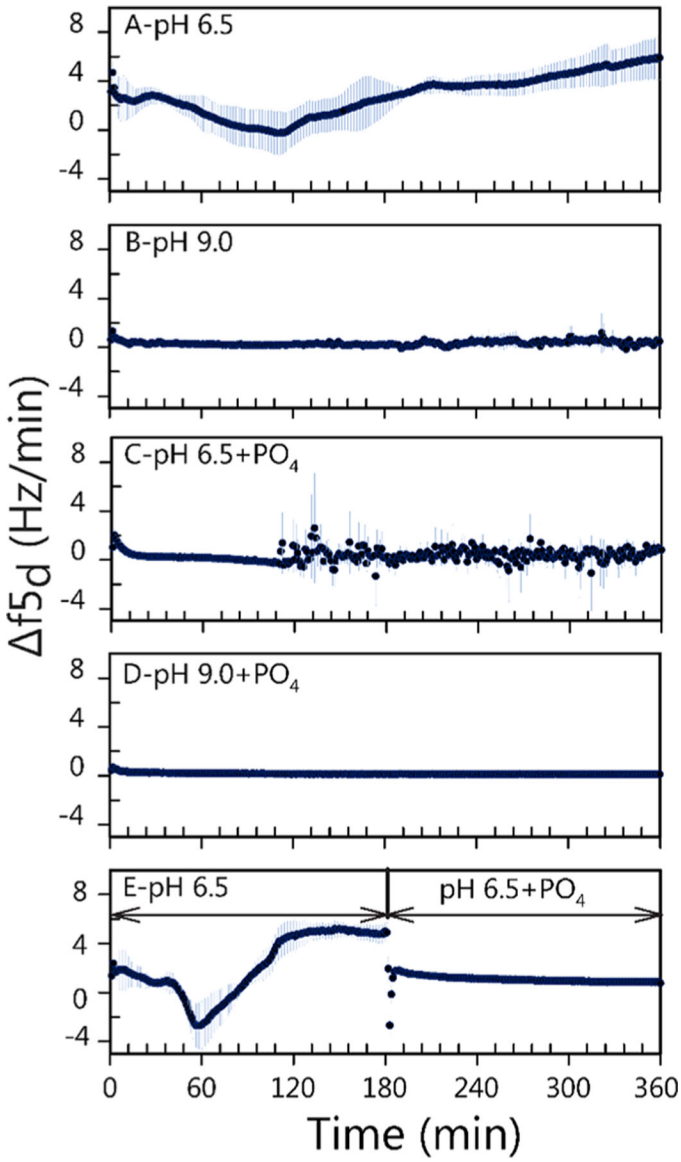

Figure 1.

Distribution of change in frequency ($\Delta f5_d$) (i.e., $\Delta f5$ for each minute) at overtone number $n = 5$ for the five examined water conditions A–E (top to bottom). The light blue error bars (or sometimes light blue band) indicate standard deviation for the three replicate copper sensors.

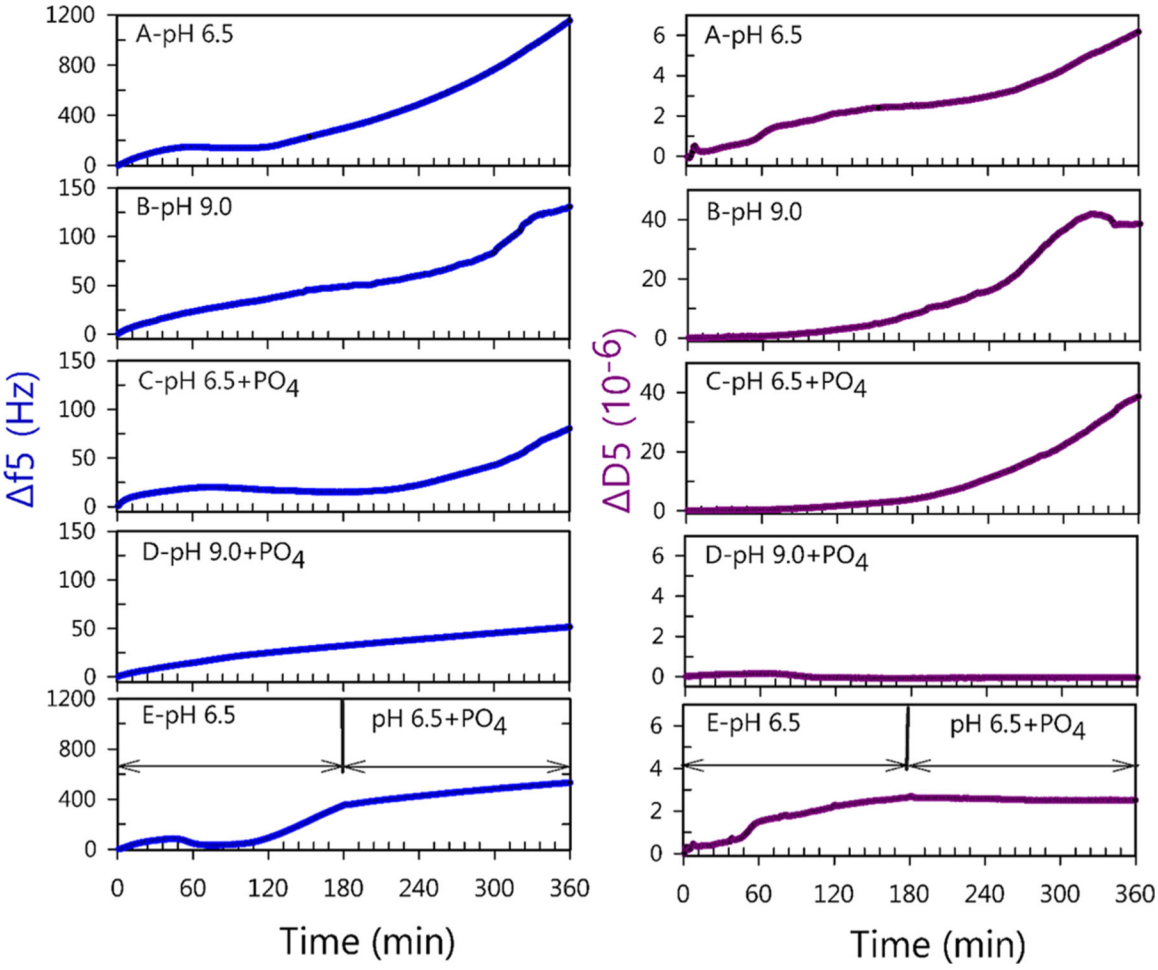

Figure 2.

Representative (i.e., one of the triplicates for each water condition) changes in frequency (left, Δf5) and changes in dissipation (right, ΔD5) as a function of experimental time at overtone number $n = 5$ for the five examined water conditions A–E (top to bottom).

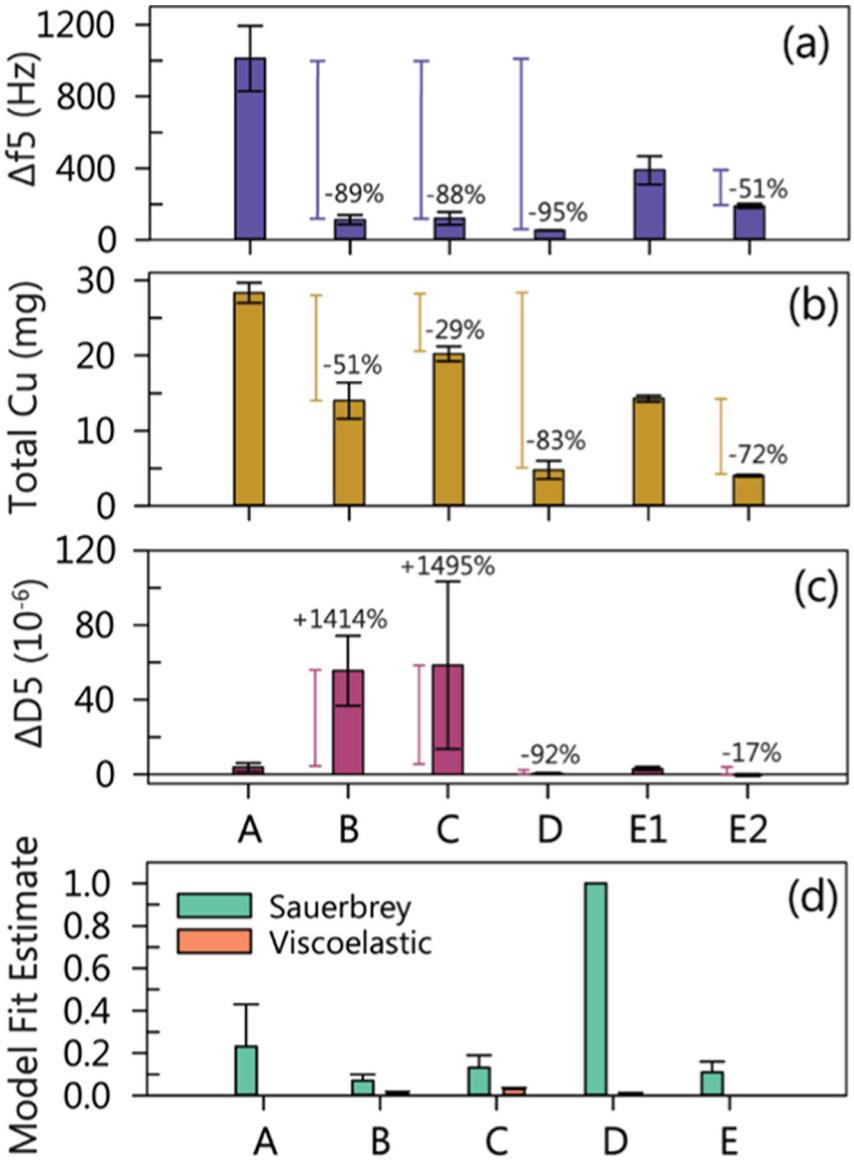

Figure 3.

Average changes in frequency (Δf5) (a), average total copper release (b), average changes in dissipation (ΔD5) (c), and model fit estimate of Sauerbrey and viscoelastic models (d) for conditions A–E. The error bars indicate a standard deviation of triplicate sensors The numbers at the top of bars B (pH 9.0 water), C (pH 6.5 + PO_4 water), and D (pH 9.0 + PO_4 water) represented the percentage changes compared to bar A (pH 6.5 water); the number at the top of bar E2 (pH 6.5 + PO_4 water in condition E) represented the percentage change compared to E1 (pH 6.5 water in condition E). Positive numbers indicated an increase and negative numbers indicated a decrease.

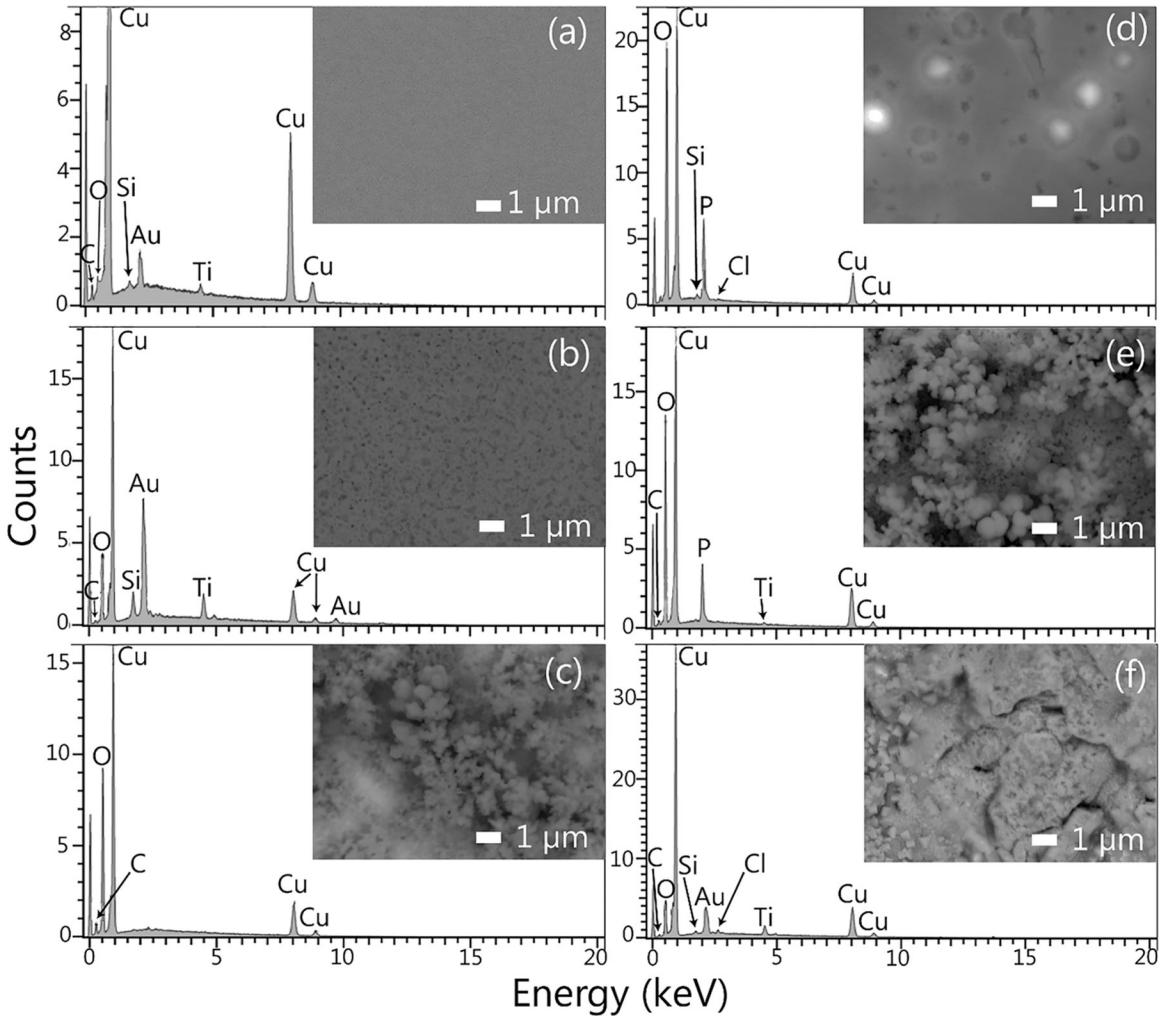

Figure 4.

FESEM images under 10,000× magnification, and examples of additional EDS results for a new sensor (a), condition A baseline water (b), condition B pH 9.0 water (c), condition C pH 6.5 + PO_4 water (d), condition D pH 9.0 + PO_4 water (e), and condition E pH 6.5_pH 6.5 + PO_4 water (f).

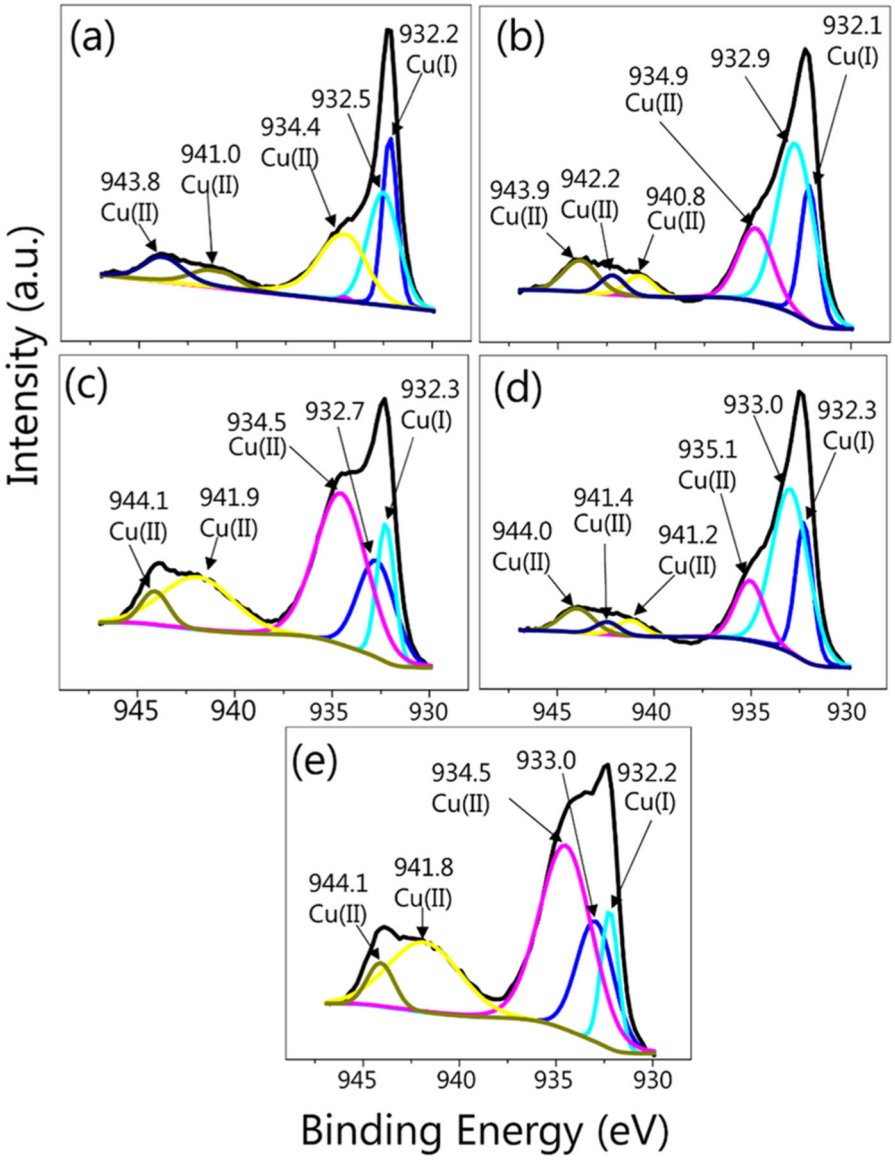

Figure 5.

XPS analyses of the primary functional sites and the surface valence states of copper (Cu 2p3/2) for a representative experimental copper sensor for condition A baseline water (a), condition B pH 9.0 water (b), condition C pH 6.5 + PO_4 water (c), condition D pH 9.0 + PO_4 water (d), and condition E pH 6.5_pH 6.5 + PO_4 water (e). The XPS analysis (conducted by the manufacturer) of a representative new copper sensor is included in the Supporting Information SI-3.